Adaptive control-based voltage regulation of a magnetically coupled multiport dc-dc converter for electrified vehicles applications

Josep M. Olm, Enric Fossas, Victor Repecho, Arnau Dòria-Cerezo and Robert Griñó
Institute of Industrial and Control Engineering
Universitat Politècnica de Catalunya
Barcelona, Spain
{josep.olm,enric.fossas,victor.repecho.del,arnau.doria,roberto.grino}@upc.edu

***Abstract*—This paper presents an adaptive control-based strategy to regulate the output voltage of a a magnetically coupled multiport dc-dc converter aimed at automotive applications. The proposed algorithm renders robustness to resistive load uncertainty and to the presence of unknown constant power loads. The theoretical analysis, which uses Lyapunov stability theory, is validated via realistic numerical simulations.**

***Index Terms*—Multiport dc-dc converter, adaptive control, automotive applications**

I. Introduction

A major increase in the use of electrified systems is seen as a viable option by OEMs (Original Equipment Manufacturers) to face the current main challenges in the automotive sector, namely, CO_2 reduction, performance enhancement, and security improvements [1], [2].

However, this entails additional issues on on-board dc microgrids, mainly related to to stability, in particular, to the connection of constant power loads (CPLs), robustness and efficiency.

Aiming at size and weight reduction, this article proposes a dc multi-bus architecture composed by a single storage element and capable of delivering the most commonly used voltages in automotive applications: 400 V for the power train [3], [4], and 48V and 12V, for auxiliary devices, see Figure 1.

The dc buses are connected by a magnetically coupled multiport dc-dc converter (400/48/12V dc). This type of dc-dc power converters are being used not only for automotive applications [5], but also in electric aircrafts [6], satellites [7], energy management systems [8], and dc grids [9], among others.

So far, the reported techniques on the control of magnetically coupled dc-dc converters are based on a linear approximated model and encompass classical PI controllers [6], [10], PI controllers based on the Generalized State-Space Averaging (GSSA) decomposition [11], decoupling methods [12], [13] and compensators like a two-pole one-zero compensator [14] and a three-pole two-zero compensator [15].

The adaptive control-based strategy presented in this paper considers the inherent nonlinearities of the model and provides energy management among the dc buses of the multiport converter, as well as ac/dc charging functionalities. Essentially, the control action is firstly transformed using a nonlinear change of variables, and an adaptive controller rendering asymptotic voltage regulation and robustness to resistive load disturbances and presence of uncertain CPLs is subsequently proposed. The stability results are derived using LaSalle's invariance principle. Finally, the control transformation is inverted using a linear approximation, which does not entail a significant performance decay. Realistic numerical simulations validate the proposal.

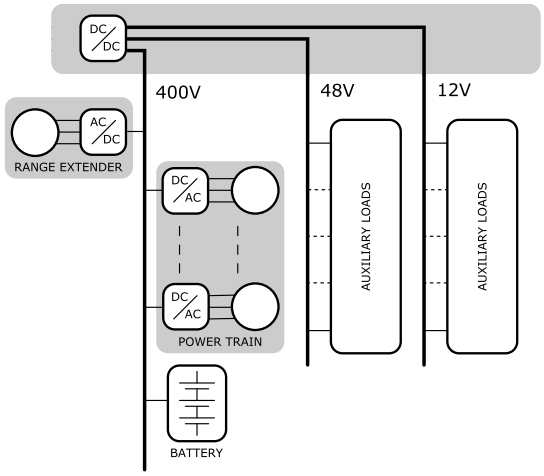

Fig. 1. Scheme of a dc-dc multi-port converter.

The paper is organized as follows. The mathematical model of the multiport dc-dc converter is presented in Section II. The adaptive controller is proposed in Section III. Simulation results are collected in Section IV and, finally, conclusions and comments on further research lines are drawn in Section V.

II. Mathematical model

A generic magnetically coupled multiport dc-dc converter is shown in Figure 2. It is composed of an n-port high frequency transformer with a full-bridge converter and a capacitor in each port side, with the subindex $k \in \{1, 2, \ldots, n\}$ indicating the

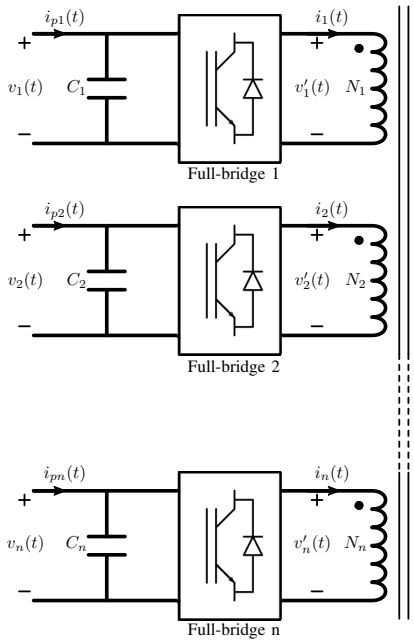

Fig. 2. Multiport dc-dc converter.

port number. DC voltages and currents are denoted by v_k, i_{pk}, C_k stand for the capacities, v_k', i_k are the high frequency voltages and currents in the transformer, and N_k are the number of coils in each winding. Following the behavioural approximation in [16], the dc voltage dynamics answer to

$$C_k \dot{v}_k = i_{pk} - \frac{1}{\omega_1} \sum_{l=1, l\neq k}^{n} \frac{v_l}{\alpha_{kl} L'_{kl}} \delta_{kl} \left(1 - \frac{|\delta_{kl}|}{\pi}\right), \quad (1)$$

where $\omega_1 = \frac{2\pi}{T}$ is the fundamental frequency of the periodic voltages and currents in the transformer, α_{kl} is the transformer turn ratio of the k-th port with respect to the l-th port, L'_{kl} is the meshed-transformed linking inductance between port k and any l-th port, and $\delta_{kl} = \theta_l - \theta_k$ is the difference between the phase shifts of the modulated voltages.

Let us consider a three-port dc bus system: a high voltage dc bus, with nominal value 400 V, and two low voltage buses, with nominal values 48 V and 12 V. The voltage at the 400 V bus is assumed constant (because of the usual high capacity battery in these buses), while the other buses have several load connections. Setting the phase shift for port 1 as the reference, i.e., $\theta_1 = 0$, the system dynamics answer to

$$\begin{aligned} C_2 \dot{v}_2 = &- \frac{v_2}{R_2} - \frac{P_2}{v_2} + \frac{E_1}{\omega_1 \alpha_{12} L'_{12}} \theta_2 \left(1 - \frac{|\theta_2|}{\pi}\right) + \\ &- v_3 \frac{1}{\omega_1 \alpha_{23} L'_{23}} (\theta_3 - \theta_2) \left(1 - \frac{|\theta_3 - \theta_2|}{\pi}\right) \quad (2a) \\ C_3 \dot{v}_3 = &- \frac{v_3}{R_3} - \frac{P_3}{v_3} + \frac{E_1}{\omega_1 \alpha_{13} L'_{13}} \theta_3 \left(1 - \frac{|\theta_3|}{\pi}\right) + \\ &+ v_2 \frac{1}{\omega_1 \alpha_{32} L'_{32}} (\theta_3 - \theta_2) \left(1 - \frac{|\theta_3 - \theta_2|}{\pi}\right), \quad (2b) \end{aligned}$$

where v_2, v_3 are the voltages of the 48 V bus and the 12 V bus, respectively, while the phase shifts in ports 2 and 3, i.e. θ_2, θ_3, are the control variables, with $\theta_k \in \left[-\frac{\pi}{2}, \frac{\pi}{2}\right]$, $k \in \{2, 3\}$.

III. Adaptive control algorithm

The control goal is to regulate the dc voltages v_2, v_3 to the reference values, $v_2^* = 48$ V and $v_3^* = 12$ V, in the face of resistive load and CPL variations in the buses, represented by R_k and P_k. The bus voltages are assumed to be measurable.

Let

$$\begin{aligned} f_k(\theta_k) &= \frac{E_1}{\omega_1 \alpha_{1k} L'_{1k}} \theta_k \left(1 - \frac{|\theta_k|}{\pi}\right), \quad k = 2, 3 \\ g(\theta_2, \theta_3) &= (\theta_3 - \theta_2) \left(1 - \frac{|\theta_3 - \theta_2|}{\pi}\right), \end{aligned}$$

and $\lambda_k = (\omega_1 \alpha_{kl} L'_{kl})^{-1}$, $k, l = 2, 3$, $k \neq l$; let also $G_k = R_k^{-1}$, $k = 2, 3$ denote the conductances in ports 2 and 3. Then, (2) becomes:

$$C_2 \dot{v}_2 = -G_2 v_2 - \frac{P_2}{v_2} + f_2(\theta_2) - \lambda_2 v_3 g(\theta_2, \theta_3) \quad (3a)$$

$$C_3 \dot{v}_3 = -G_3 v_3 - \frac{P_3}{v_3} + f_3(\theta_3) + \lambda_3 v_2 g(\theta_2, \theta_3). \quad (3b)$$

Let us now consider the change of control variables

$$u_2 = f_2(\theta_2) - \lambda_2 v_3^* g(\theta_2, \theta_3) \quad (4a)$$

$$u_3 = f_3(\theta_3) + \lambda_3 v_2^* g(\theta_2, \theta_3), \quad (4b)$$

which, denoting $u = (u_2, u_3)^\top$, $\theta = (\theta_2, \theta_3)^\top$, can be written in compact form as $u = h(\theta)$, with $h : \left[-\frac{\pi}{2}, \frac{\pi}{2}\right]^2 \longrightarrow \mathbb{R}^2$ appropriately defined componentwise using (4a),(4b). Finally, let us assume that h is invertible in a region of interest, and define $H = g \circ h^{-1}$. Then, in the error variables $e_k = v_k - v_k^*$, $k = 2, 3$, (3) boils down to

$$C_2 \dot{e}_2 = -G_2 (e_2 + v_2^*) - \frac{P_2}{e_2 + v_2^*} - \lambda_2 e_3 H(u) + u_2 \quad (5a)$$

$$C_3 \dot{e}_3 = -G_3 (e_3 + v_3^*) - \frac{P_3}{e_3 + v_3^*} + \lambda_3 e_2 H(u) + u_3. \quad (5b)$$

Proposition 1. *Let $G_k, P_k \geq 0$, $k = 2, 3$, in (5) be constant, unknown conductances and CPLs, respectively, and let $\hat{G}_k, \hat{P}_k$, denote their estimated values. Then, the adaptive control law*

$$u_k = \hat{G}_k (e_k + v_k^*) + \frac{\hat{P}_k}{e_k + v_k^*} - \gamma_k e_k, \quad (6a)$$

$$\dot{\hat{G}}_k = -\frac{\mu_k}{\lambda_k} e_k (e_k + v_k^*), \quad (6b)$$

$$\dot{\hat{P}}_k = -\frac{\nu_k e_k}{\lambda_k (e_k + v_k^*)}, \quad (6c)$$

with $\gamma_k, \mu_k, \nu_k \in \mathbb{R}^+$, $k = 2, 3$, makes the closed-loop system (5),(6) locally stable and $e_k \to 0$, $k = 2, 3$, when $t \to +\infty$.

Proof. Let $\Delta G_k = G_k - \hat{G}_k$, $\Delta P_k = P_k - \hat{P}_k$, $k = 2, 3$, denote the estimation errors for conductances and CPLs. As

G_k, P_k are assumed constant, it is immediate that, for $k = 2, 3$, $\dot{\Delta} G_k = -\dot{\hat{G}}_k$, $\dot{\Delta} P_k = -\dot{\hat{P}}_k$. Therefore, (5),(6) reads as:

$$C_2 \dot{e}_2 = -\Delta G_2 \left(e_2 + v_2^*\right) - \frac{\Delta P_2}{e_2 + v_2^*} - \lambda_2 e_3 H(u) - \gamma_2 e_2 \tag{7a}$$

$$C_3 \dot{e}_3 = -\Delta G_3 \left(e_3 + v_3^*\right) - \frac{\Delta P_3}{e_3 + v_3^*} + \lambda_3 e_2 H(u) - \gamma_3 e_3 \tag{7b}$$

$$\dot{\Delta} G_k = \frac{\mu_k}{\lambda_k} e_k \left(e_k + v_k^*\right), \quad k = 2, 3 \tag{7c}$$

$$\dot{\Delta} P_k = \frac{\nu_k e_k}{\lambda_k \left(e_k + v_k^*\right)}, \quad k = 2, 3. \tag{7d}$$

Notice that the auxiliary function

$$V = \frac{1}{2} \sum_{k=2}^{3} \left(\frac{C_k}{\lambda_k} e_k^2 + \frac{1}{\mu_k} \Delta G_k^2 + \frac{1}{\nu_k} \Delta P_k^2 \right)$$

is positive definite, while $\dot{V}$ is negative semidefinite:

$$\dot{V} = -\frac{\gamma_2}{\lambda_2} e_2^2 - \frac{\gamma_3}{\lambda_3} e_3^2 \leq 0.$$

Moreover, the subset of $\mathbb{R}^6$ where $\dot{V} = 0$ is

$$\Omega_R := \left\{ (0, 0, \Delta G_2, \Delta G_3, \Delta P_2, \Delta P_3), \ \Delta G_k, \Delta P_k \in \mathbb{R} \right\},$$

while the largest invariant set within Ω_R is

$$\Omega := \left\{ (0, 0, \Delta G_2^*, \Delta G_3^*, \Delta P_2^*, \Delta P_3^*), \Delta P_k^* = -\Delta G_k^* v_k^{*2} \right\}.$$

Then, La Salle's invariance principle ensures that, locally, the trajectories of (7) tend to Ω for $t \to +\infty$. □

Remark 1. *Notice that, although the control law* (6) *yields asymptotic voltage regulation, the fact that the equilibrium values* $\Delta G_k^*, \Delta P_k^*$, $k = 2, 3$, *are not guaranteed to be zero does not allow to identify the real values of conductances and CPLs.*

The control law transformation (4) involves absolute value terms. In order to carry out the inversion, i.e. to obtain $\theta = H(u)$, it is important to realize that the $\mathbb{R}^3$ surfaces defined in (4) reveal a linear dependence in the region of interest, namely, $u_k \in [0, 50]$A, $k = 2, 3$, as shown in Figure 3.

Therefore, the inversion will be performed from the linear approximation of the change of variables (4), namely,

$$u_2 \approx \beta_2 \theta_2 - \lambda_2 v_3^* \left(\theta_3 - \theta_2\right) \tag{8a}$$

$$u_3 \approx \beta_3 \theta_3 + \lambda_3 v_2^* \left(\theta_3 - \theta_2\right), \tag{8b}$$

with $\beta_k = E_1 \left(\omega_1 \alpha_{1k} L'_{1k}\right)^{-1}$, $k = 2, 3$. Then:

$$\theta_2 \approx \frac{\left(\lambda_3 v_2^* + \beta_3\right) u_2 + \lambda_2 v_3^* u_3}{\lambda_3 \beta_2 v_2^* + \lambda_2 \beta_3 v_3^* + \beta_2 \beta_3} \tag{9a}$$

$$\theta_3 \approx \frac{\lambda_3 v_2^* u_2 + \left(\lambda_2 v_3^* + \beta_2\right) u_3}{\lambda_3 \beta_2 v_2^* + \lambda_2 \beta_3 v_3^* + \beta_2 \beta_3}, \tag{9b}$$

where the control actions u_k are defined in (6).

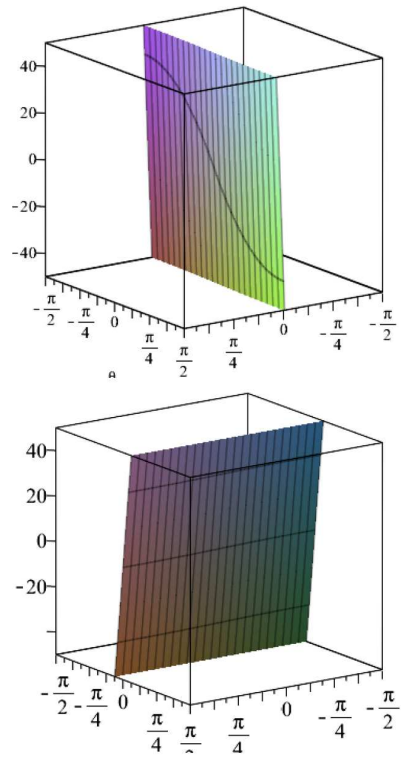

Fig. 3. $u = H(\theta)$. Top: u_2; bottom: u_3.

IV. Simulation results

The simulations have been carried out with Matlab-Simulink, and the DC converter is modelled with SimScape. The solver uses a 10^{-8} fixed step size Runge-Kutta ode4 integration algorithm. The converter model includes switching and conduction losses in the power switches, resistive losses in the transformer windings, and reactive components. The branches of the full-bridge converters incorporate a 1μs dead time to avoid bus voltage short circuits. First order filters with unitary gain and 2ms time constant are placed in the feedback loops. System and control parameters are in Table I.

TABLE I
Parameters for system (2)

E_1	400 V	ω_1	$2\pi \cdot 40.0 \cdot 10^3$ rad/s
C_2	200 μF	C_3	600 μF
α_{12}	0.125	α_{13}	0.033
α_{23}	0.267	α_{32}	3.75
L'_{12}	1.27 μH	L'_{13}	0.53 μH
L'_{23}	0.58 μH	L'_{32}	34.6 μH
γ_2	4800	γ_3	$4.8 \cdot 10^4$
μ_2	51327	μ_3	61.327
ν_2	$1.283 \cdot 10^9$	ν_3	$1.5332 \cdot 10^8$

Piecewise constant profiles for the resistive loads have been used:

$$R_2 = \begin{cases} 5\ \Omega & t \in [0, 0.03) \cup [0.05, 0.1)\ s \\ 1\ \Omega & t \in [0.03, 0.05)\ s \end{cases}$$

$$R_3 = \begin{cases} 10\ \Omega & t \in [0, 0.04) \cup [0.06, 0.1) s \\ 3\ \Omega & t \in [0.04, 0.06)\ s. \end{cases}$$

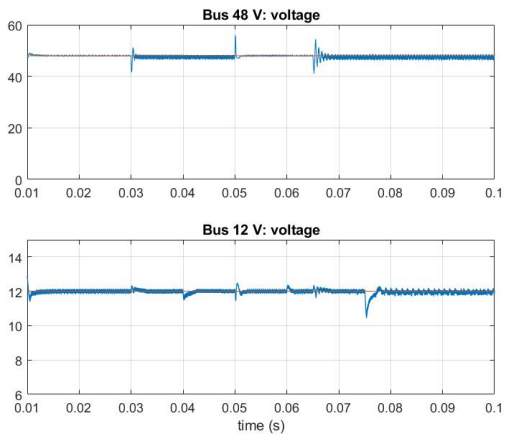

Fig. 4. Bus voltage (blue) and voltage reference (red). Top: $48V$ bus; bottom: $12V$ bus.

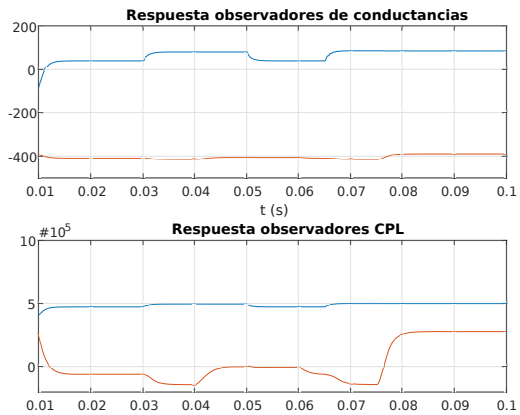

Fig. 6. Observers. Top: estimated conductances $\hat{G}_2$ (blue), $\hat{G}_3$ (red); bottom: estimated CPLs $\hat{P}_2$ (blue), $\hat{P}_3$ (red).

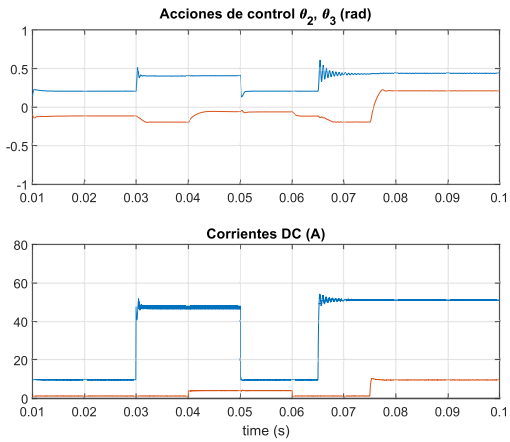

Fig. 5. Top: control actions θ_2 (blue), θ_3 (red) in radiants; bottom: output currents $-i_{p2}$ (blue), $-i_{p3}$ (red) in Ampères.

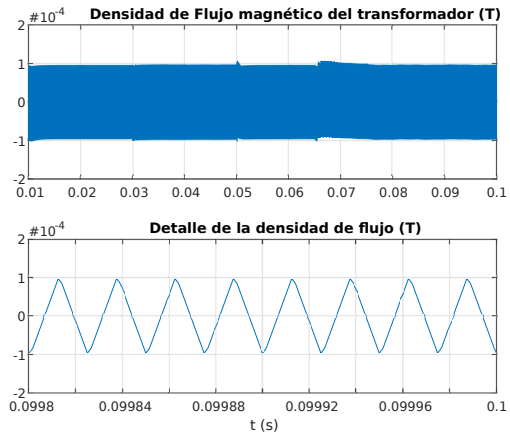

Fig. 7. Top: flux density at the core of the transformer; bottom: detail.

In turn, piecewise constant CPL profiles connected via first order filters with time constant 0.1ms have also been used:

$$P_2 = \begin{cases} 0 & t \in [0, 0.065) \text{ s} \\ 2\text{kW} & t \in [0.065, 0.1) \text{ s} \end{cases}$$

$$P_3 = \begin{cases} 0 & t \in [0, 0.075) \text{ s} \\ 100\text{W} & t \in [0.075, 0.1) \text{ s} \end{cases}$$

The stability and robustness features of the control design are shown in Figure 4, which portrays the bus voltages tracking their corresponding references. The top part of Figure 5 shows the control action variables reacting in a bounded way to cancel out the effect of the sudden load and CPL changes in the bus voltages. The output currents, $-i_{p2}, -i_{p3}$ (recall Figure 2), are displayed in the bottom part. The estimated values of the conductances and CPLs are depicted in Figure 6: according to Proposition 1 and Remark 1, all the signals stabilize but not at the real values. Moreover, the flux density at the core of the transformer depicted in Figure 7 guarantees that there are no saturation issues.

Finally, it turns out that adding a $5\mu H$ inductance in series with the primary winding with no update of the control parameters, produces essentially the same outcome. This result further illustrates the controller robustness. For the sake of brevity, the plots corresponding to this last case are omitted.

V. Conclusions

An adaptive controller was designed for a magnetically coupled dc-dc converter providing asymptotic voltage regulation and robustness in the face of resistive load uncertainty and presence of CPLs. A key role in the control design was played by a nonlinear control transformation that was subsequently inverted using a linear approximation with no significant performance loss. Realistic numerical simulations confirmed the theoretical analysis.

Acknowledgment

The work was partially supported by the Government of Spain through the *Agencia Estatal de Investigación* Project DPI2017-85404-P and by the *Generalitat de Catalunya* through the Project 2017 SGR 872.

REFERENCES

[1] "Use of new energies in road transport," European Green Vehicles Initiative. PPP, Tech. Rep., 2013.

[2] "Hybrid and electric vehicles - the electric drive commutes," International Energy Agency, Tech. Rep., 2016.

[3] C. Chan, "The state of the art of electric, hybrid, and fuel cell vehicles," *Proc. of the IEEE*, vol. 95, no. 4, pp. 704–718, 2007.

[4] O. Coppin, "From 12+12V to 48V: a new road map for hybridization," in *Proc. Engine Expo 2016*, 2016.

[5] B. Farhangi and H. Toliyat, "Modeling and analyzing multiport isolation transformer capacitive components for onboard vehicular power conditioners," *IEEE Trans. on Industrial Electronics*, vol. 62, no. 5, pp. 3134–3142, 2015.

[6] B. Karanayil, M. Ciobotaru, and V. Agelidis, "Power flow management of isolated multiport converter for more electric aircraft," *IEEE Trans. on Power Electronics*, vol. 32, no. 7, pp. 5850–5861, 2017.

[7] Z. Qian, "Modeling and design of multi-port dc/dc converters," Ph.D. dissertation, University of Central Florida, 2010.

[8] H. Tao, J. Duarte, and M. Hendrix, "Three-port triple-half-bridge bidirectional converter with zero-voltage switching," *IEEE Trans. on Power Electronics*, vol. 23, no. 2, pp. 782–792, 2008.

[9] H. Matsuo, W. Lin, F. Kurokawa, T. Shigemizu, and N. Watanabe, "Characteristics of the multiple-input DC-DC converter," *IEEE Trans. on Industrial Electronics*, vol. 51, no. 3, pp. 625 – 631, 2004.

[10] V. Jakka, A. Shukla, and G. Demetriades, "Dual-transformer-based asymmetrical triple-port active bridge (DT-ATAB) isolated DC–DC converter," *IEEE Trans. on Industrial Electronics*, vol. 64, no. 6, pp. 4549–4560, 2017.

[11] Z. Li, Y. Wang, L. Shi, J. Huang, Y. Cui, and W. Lei, "Generalized averaging modeling and control strategy for three-phase dual-active-bridge DC-DC converters with three control variables," in *Proc. IEEE Applied Power Electronics Conference and Exposition*, 2017.

[12] C. Zhao, S. Round, and J. Kolar, "An isolated three-port bidirectional DC-DC converter with decoupled power flow management," *IEEE Trans. on Power Electronics*, vol. 23, no. 5, pp. 2443–2453, 2008.

[13] K. Xiangli, S. Li, and K. Smedley, "Decoupled pwm plus phase-shift control for a dual-half-bridge bidirectional dc–dc converter," *IEEE Trans. on Power Electronics*, vol. 33, no. 8, p. 7203–7213, 2018.

[14] B. Choi, W. Lim, S. Choi, and J. Sun, "Comparative performance evaluation of current-mode control schemes adapted to asymmetrically driven bridge-type pulsewidth modulated dc-to-dc converters," *IEEE Trans. on Industrial Electronics*, vol. 55, no. 5, p. 2033–2042, 2008.

[15] Z. Qian, O. Abdel-Rahman, H. Al-Atrash, and I. Batarseh, "Modeling and control of three-port DC/DC converter interface for satellite applications," *IEEE Trans. on Power Electronics*, vol. 25, no. 3, pp. 637–649, 2010.

[16] R. Griñó and A. Dòria-Cerezo, "Modelling and simulation of a magnetically coupled multiport dc-dc converter," in *Proc. 24th Int. Conf. on Emerging Technologies and Factory Automation*, 2019.